Supplement of Atmos. Chem. Phys., 25, 759–770, 2025
https://doi.org/10.5194/acp-25-759-2025-supplement

Atmospheric Chemistry and Physics
Open Access

Supplement of

Unleashing the potential of geostationary satellite observations in air quality forecasting through artificial intelligence techniques

Chengxin Zhang et al.

Correspondence to: Cheng Liu (chliu81@ustc.edu.cn)

Supplementary Text

S1. Data pre-processing

Outlier Handling

We conducted outlier handling for each GeoNet input datasets using z-scores, wherein data normalization was performed based on the mean and standard deviation. Data points exceeding a certain threshold of z-scores were discarded. The calculation formula is as follows:

$$z(x) = \frac{x - \mu_x}{\sigma_x}$$

Where x is the data value, μ_x and σ_x are the mean average and standard deviation.

Missing Value Handling

Due to meteorological factors, the GEMS dataset used in this study contains many missing values. Fig. S1 presents the overall missing ratio of GEMS satellite NO_2 retrieval for each ground pixel in 2021.

To enhance data availability, the GEMS dataset underwent imputation procedures. Various data imputation methods were employed to assess their impact on the dataset, including zero imputation, WRF data imputation, and CAMS data imputation. Specifically, missing data points were replaced with either zero or corresponding data from the WRF and CAMS datasets at the respective spatiotemporal positions. For other datasets, missing values were addressed through spatiotemporal interpolation using multidimensional linear interpolation.

Resampling

Due to variations in spatiotemporal resolutions among different datasets, it was necessary to ensure data consistency and facilitate model computation by resampling all datasets in both time and space domains. Resampling operations involved both upsampling and downsampling. Upsampling was achieved through interpolation, while downsampling was performed using local mean aggregation. Following resampling, the temporal resolution of all datasets was standardized to 1 hour, and the spatial resolution to 0.1 degrees.

Normalization

The normalization process applied here is beneficial for overcoming overfitting issues during model training and dealing with heterogeneous data of different scales, thereby potentially accelerating training speed. This process is essential for bringing each variable to a comparable scale, ensuring that each feature carries similar importance. In this study, min-max normalization was applied to all datasets. In this method, the maximum value of the data is transformed to 1, the minimum value to 0, and other values are scaled to decimals between 0 and 1. The calculation method is as follows:

$$x_n = \frac{x - x_{min}}{x_{max} - x_{min}}$$

Where x, x_{max}, x_{min} is the data value, maximum, and minimum, respectively.

S2. The definition of model performance metrics

The coefficient of determination (R^2):

$$R^2 = \frac{\sum_{i=1}^{m}(f(x_i) - \bar{y})^2}{\sum_{i=1}^{m}(y_i - \bar{y})^2}$$

The root mean square error (RMSE):

$$\sqrt{\frac{1}{n}\sum_{i=1}^{n}(\hat{y_i} - y_i)^2}$$

The mean absolute error (MAE):

$$\frac{1}{n}\sum_{i=1}^{n}|\hat{y_i} - y_i|$$

The mean absolute percentage error (MAPE):

$$\frac{1}{n}\sum_{i=1}^{n}\left|\frac{\hat{y_i} - y_i}{y_i}\right|$$

Supplementary Figures

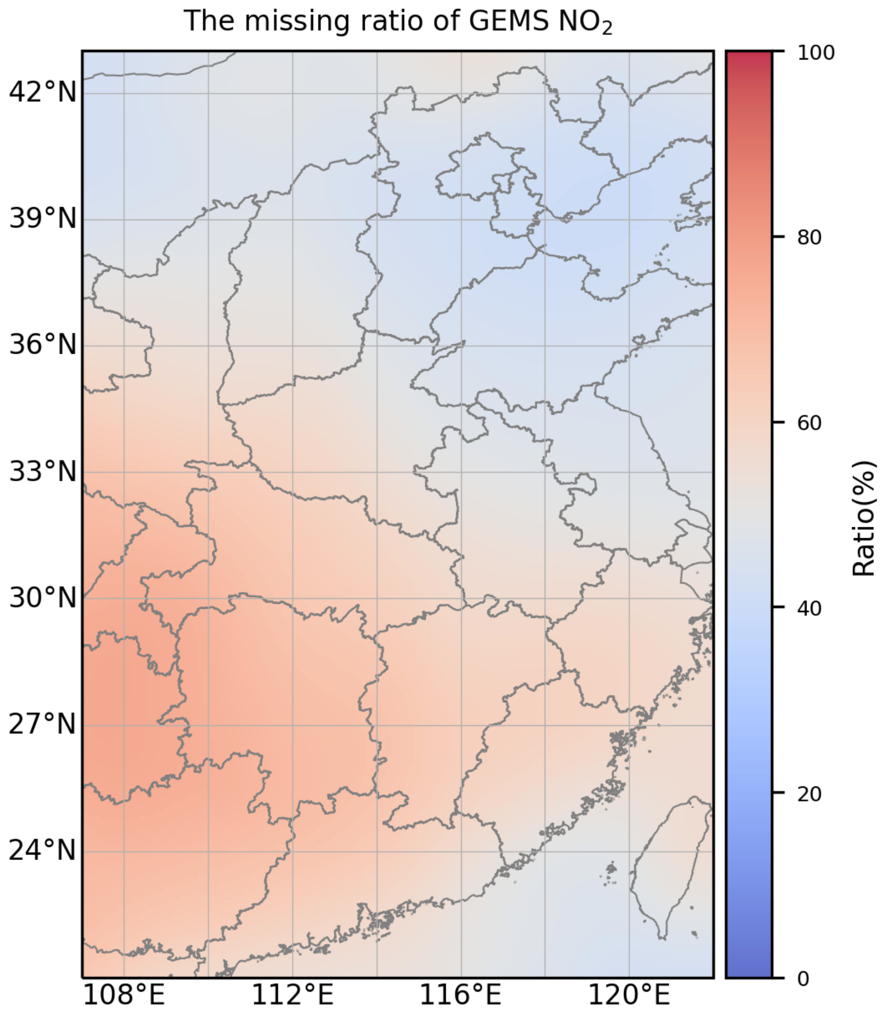

Figure S1. The ratio of missing data for hourly GEMS NO_2 retrievals over East China in 2021.

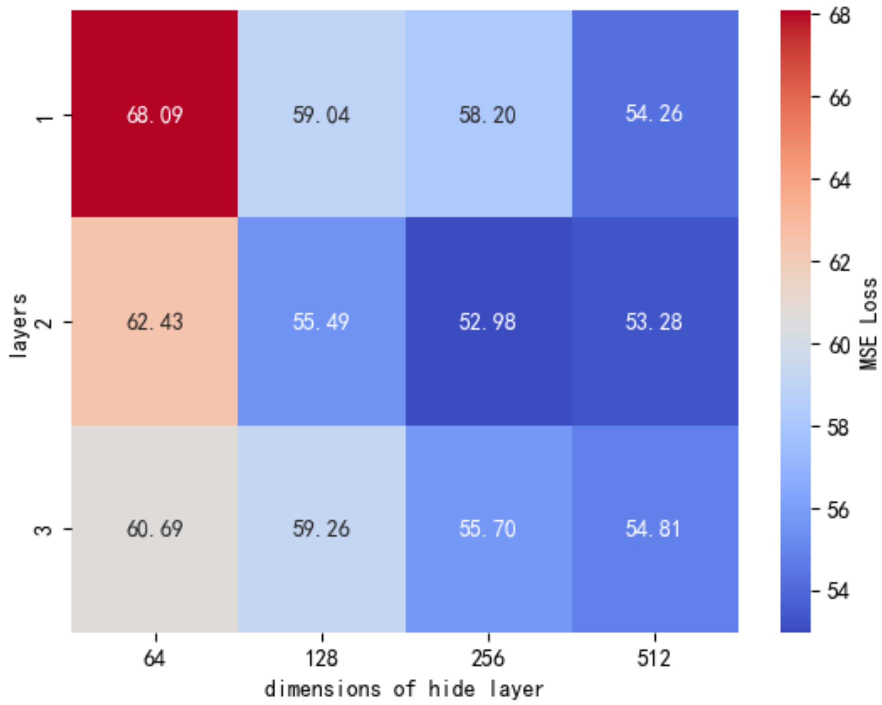

Figure S2. The influence of model hyperparameters including both ConvLSTM layers and dimensions of hide layer on the MSE loss of GeoNet prediction.

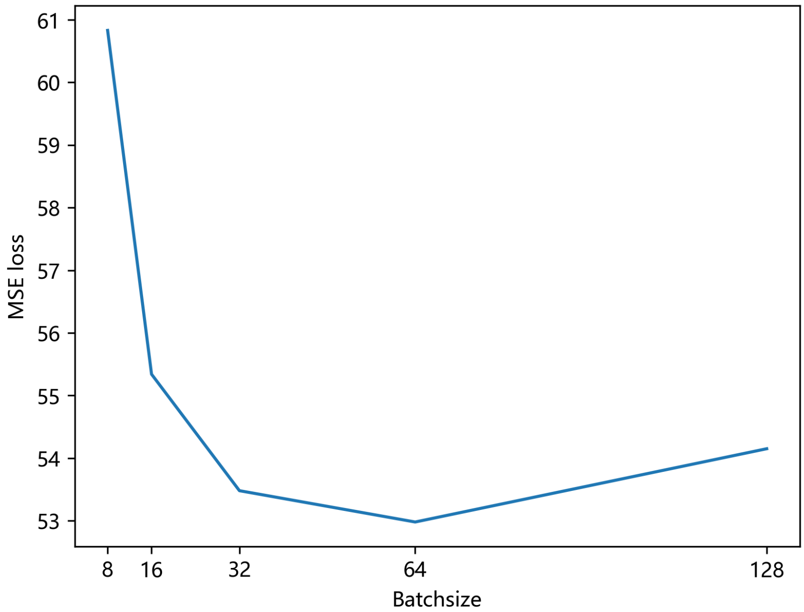

Figure S3. The impact of batch size on the MSE loss of GeoNet prediction.

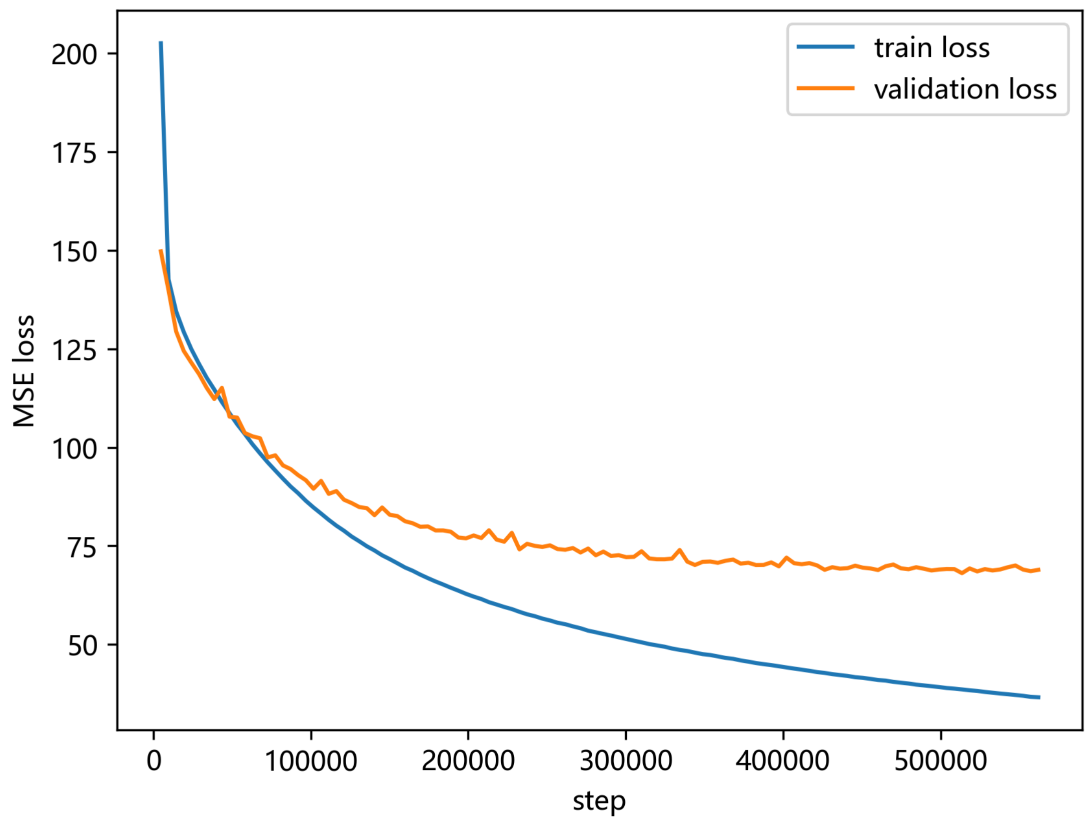

Figure S4. The learning curve of model loss in validation and training datasets for different steps.

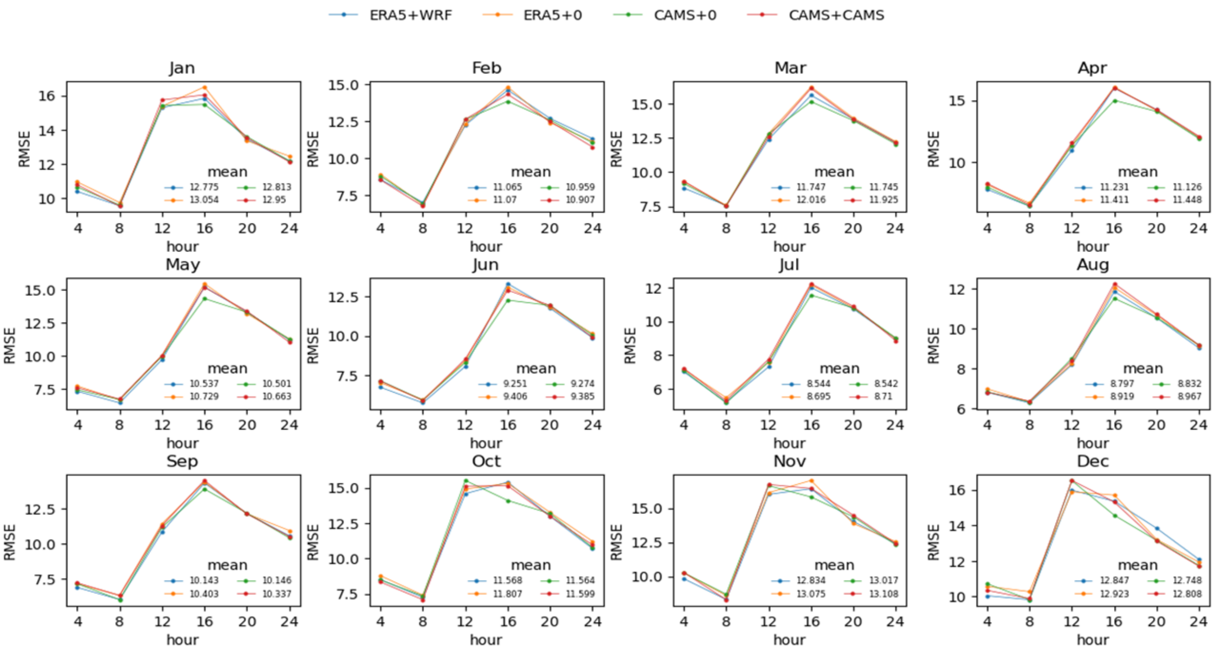

Figure S5. The RMSE of GeoNet predicted-NO_2 varys with different prediction step from t+4h to t+24h, for different months.

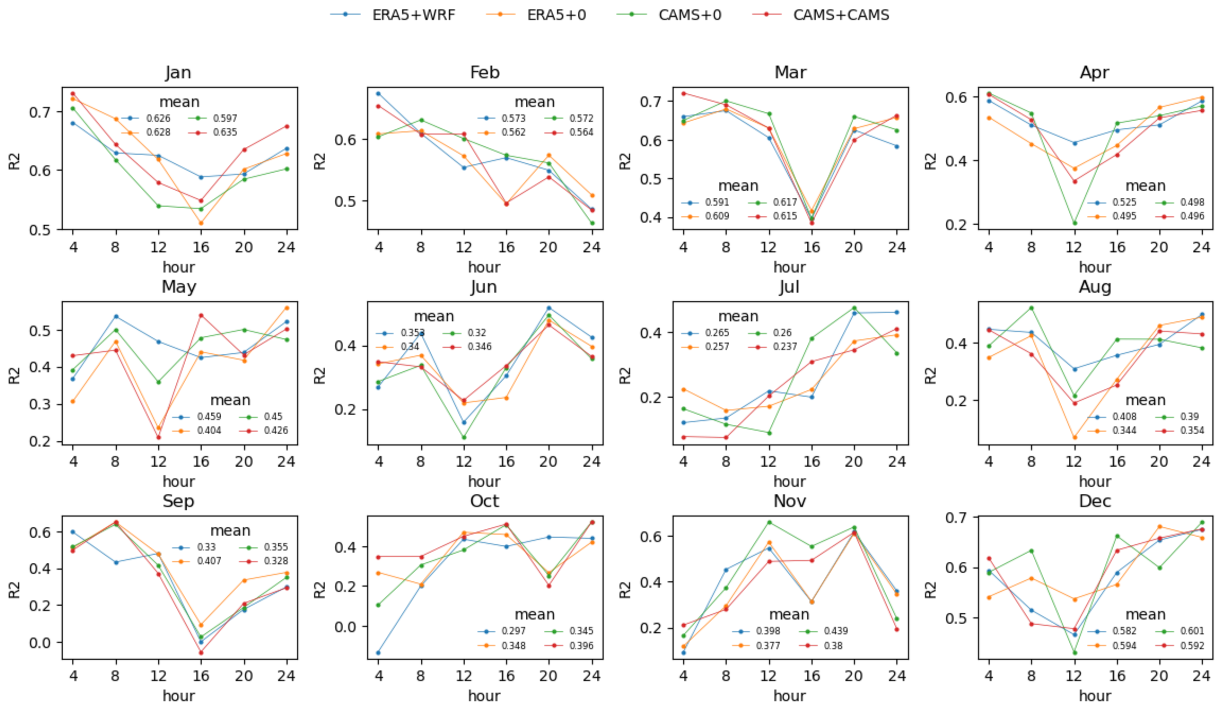

Figure S6. Similar to Fig. S5, but for R^2.

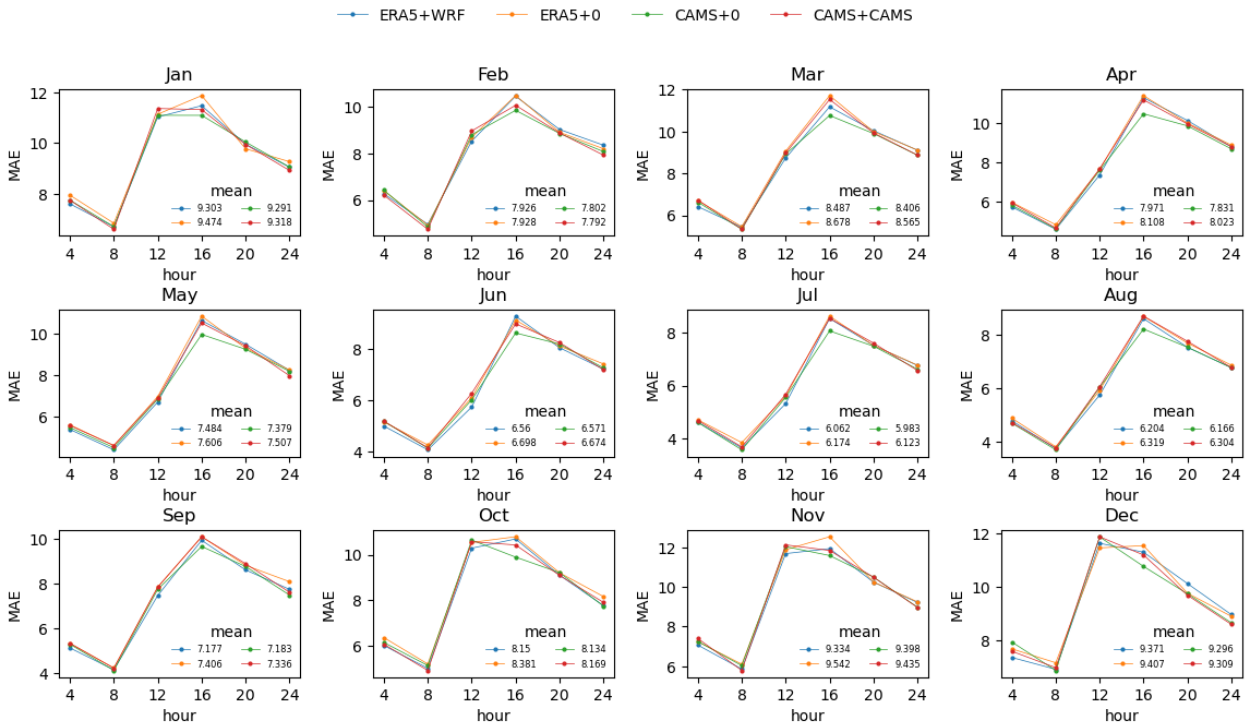

Figure S7. Similar to Fig. S5, but for MAE.

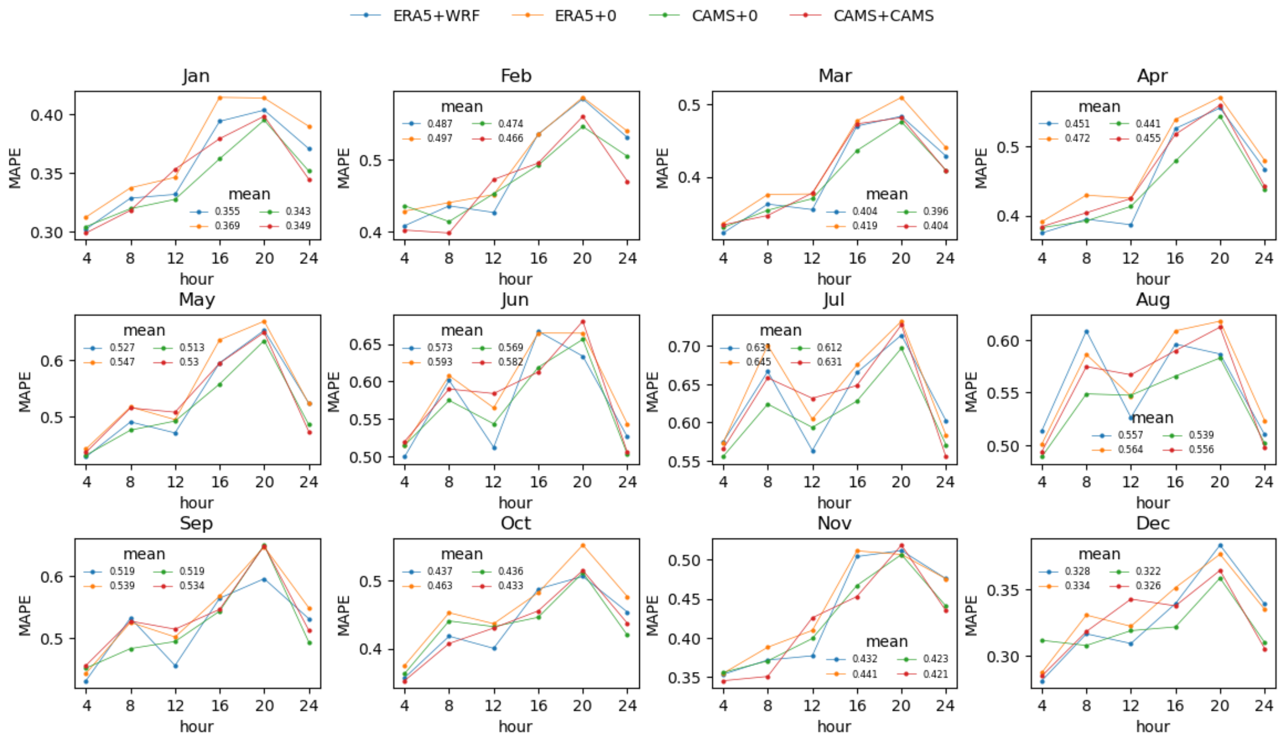

Figure S8. Similar to Fig. S5, but for MAPE.

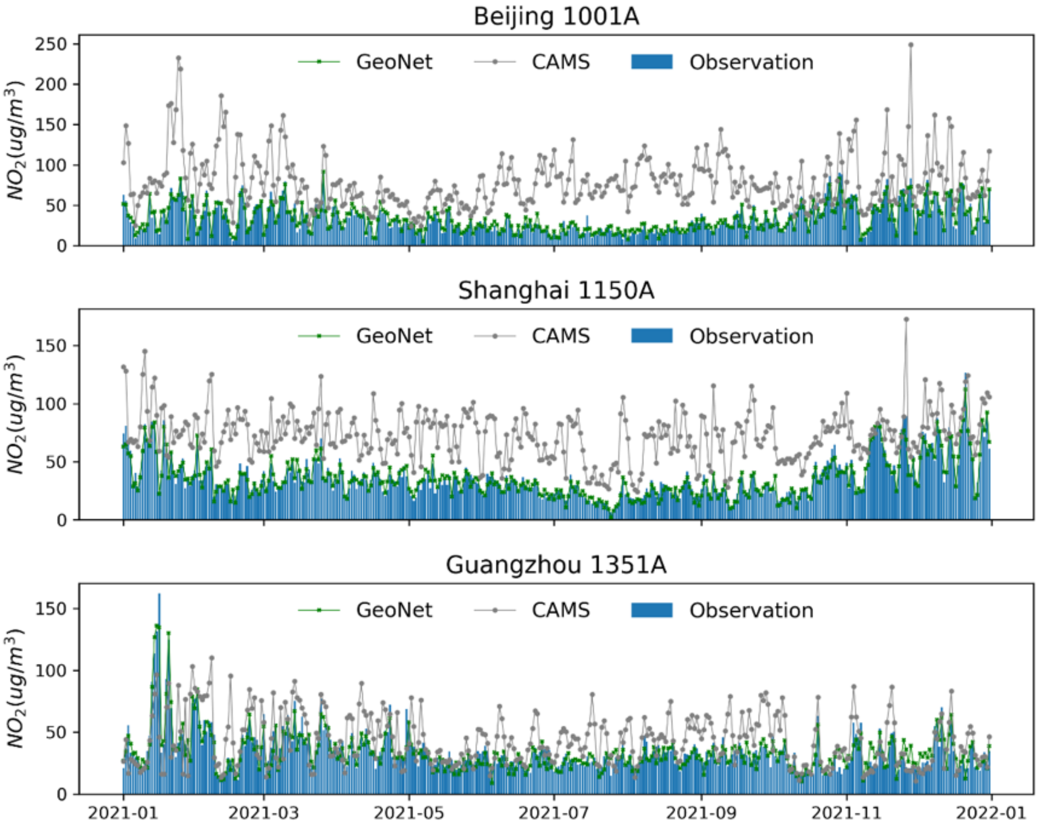

Figure S9. Time series comparison of daily t+4h prediction of surface NO_2 concentration among GeoNet and CAMS prediction, as well as the CNEMC measurements. These results are shown for one typical site in (**a**) Beijing, (**b**) Shanghai, and (**c**) Guangzhou, respectively.

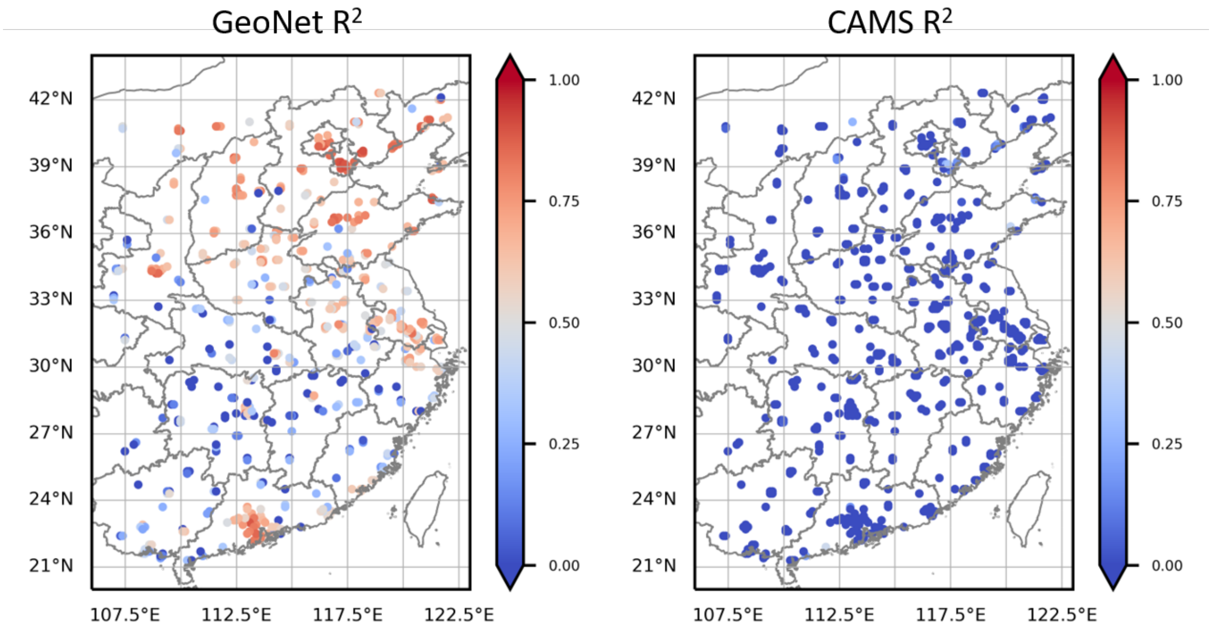

Figure S10. The site-specific Pearson's R^2 between the CNEMC measurements and NO_2 prediction by (a) GeoNet, and (b) CAMS over East China.

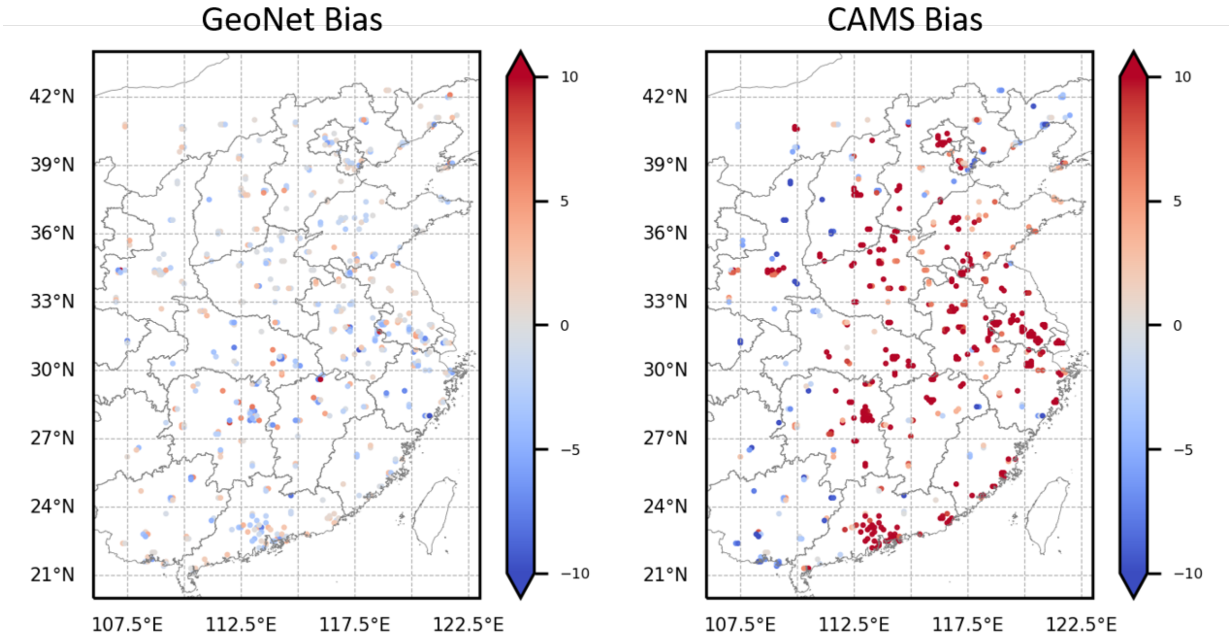

Figure S11. Similar to Fig. S10, but for RMSE.

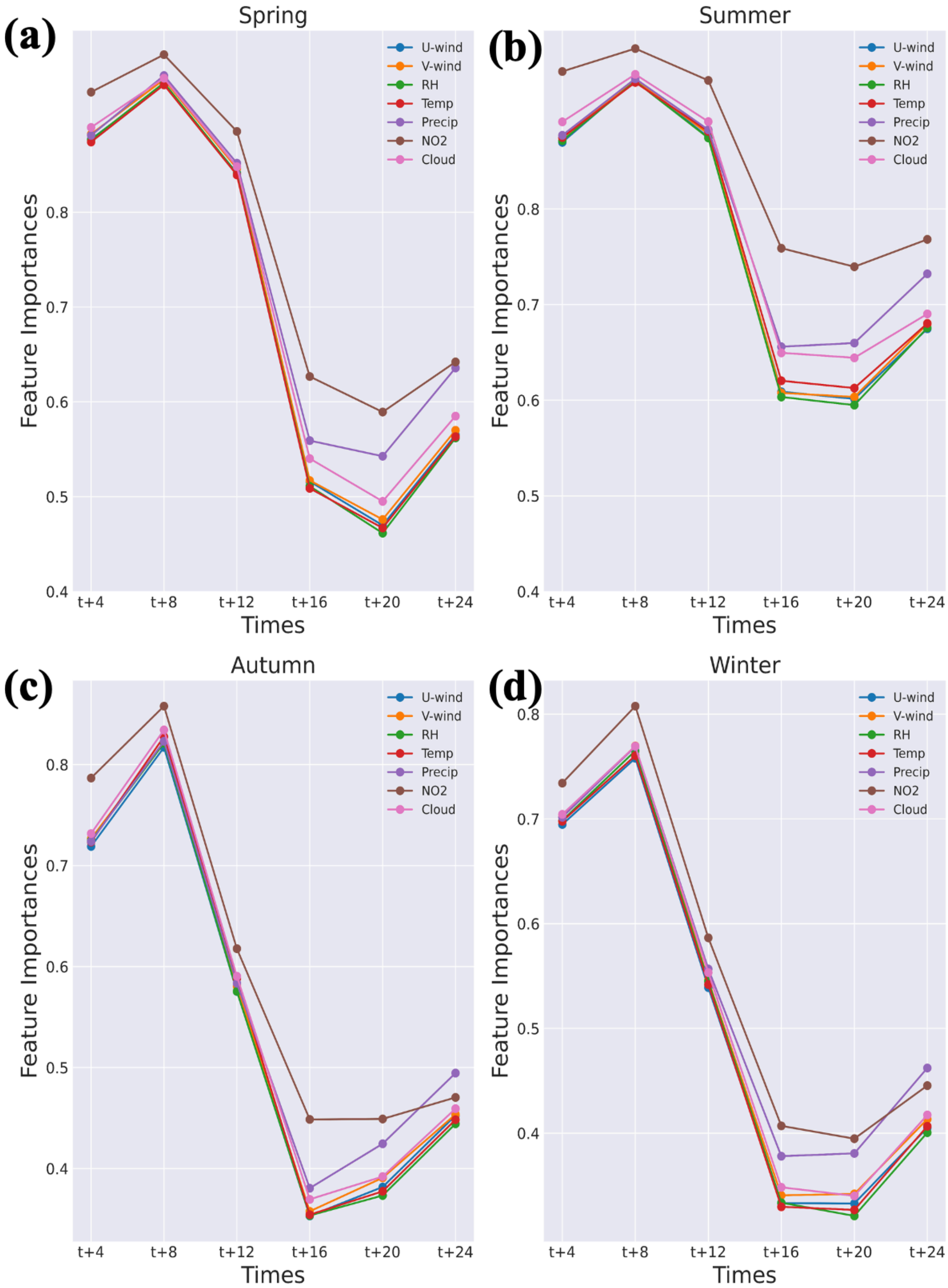

Figure S12. Similar to Fig 3a, but for different seasons, including Spring (a), Summer (b), Autumn (c), and Winter (d).